Journal of Controlled Release 308 (2019) 190–196

Contents lists available at ScienceDirect

Journal of Controlled Release

journal homepage: www.elsevier.com/locate/jconrel

In vivo quantitative molecular absorption of glycerol in human skin using coherent anti-Stokes Raman scattering (CARS) and two-photon auto-fluorescence

Barbara Sarri[a], Xueqin Chen[b], Rafaël Canonge[a], Sébastien Grégoire[b], Florian Formanek[b], Jean-Baptiste Galey[b], Anne Potter[b], Thomas Bornschlögl[b], Hervé Rigneault[a,*]

[a] Aix Marseille Univ, CNRS, Centrale Marseille, Institut Fresnel, Marseille, France
[b] L'Oréal Recherche Avancée, Aulnay-sous-bois, France

ARTICLE INFO

Keywords:
In vivo molecular cutaneous absorption
Coherent anti-Stokes Raman Scattering (CARS)
Quantitative molecular imaging
Molecular penetration pathways
Human skin

ABSTRACT

The penetration of small molecules through the human skin is a major issue for both safety and efficacy issues in cosmetics and pharmaceutic domains. To date, the quantification of active molecular compounds in human skin following a topical application uses ex vivo skin samples mounted on Franz cell diffusion set-up together with appropriate analytical methods. Coherent anti-Stokes Raman scattering (CARS) has also been used to perform active molecule quantification on ex vivo skin samples, but no quantification has been described in human skin in vivo. Here we introduce and validate a framework for imaging and quantifying the active molecule penetration into human skin in vivo. Our approach combines nonlinear imaging microscopy modalities, such as two-photon excited auto-fluorescence (TPEF) and coherent anti-Stokes Raman scattering (CARS), together with the use of deuterated active molecules. The imaging framework was exemplified on topically applied glycerol diluted in various vehicles such as water and xanthan gel. In vivo glycerol quantitative percutaneous penetration over time was demonstrated, showing that, contrary to water, the xanthan gel vehicle acts as a film reservoir that releases glycerol continuously over time. More generally, the proposed imaging framework provides an enabling platform for establishing functional activity of topically applied products in vivo.

1. Introduction

Although human skin primarily functions as a barrier to prevent or control the entry of foreign substances into the body [1], a topical delivery is attractive to pharmaceutical and cosmetic compounds as this route of administration avoids hepatic first pass and provides a constant molecular flux into the blood. Understanding [2] and predicting [3] molecular percutaneous penetration, even for small molecules [4], remains extremely difficult due to the complexity of the skin layered morphology and the variety of active metabolic processes possibly involved. Addressing this complex question would require an in vivo experimental framework capable of providing a detailed anatomical skin description together with a 3D active molecule concentration view over the time course of the experiment. This is in sharp contrast with the information provided by conventional skin bioavailability approaches such as ex vivo human skin mounted on Franz cell diffusion set-up together with validated analytical methods (such as radio-labeled compounds [5] or liquid chromatography-tandem mass spectroscopy [6]) or destructive sequential adhesive tape stripping extraction to determine active molecule concentration profile at specific time point [7].

Recently many efforts have been made to develop skin imaging modalities that use inelastic scattered light by the vibrational motions of chemical bonds [8]. Known as spontaneous Raman spectroscopy techniques, they provide sufficient chemical specificities to track active molecules in skin both in-vitro [9] and in-vivo [10]. Other label free imaging modalities such as high-frequency ultra-sound imaging [11], optical coherence tomography (OCT) [12] and multiphoton microscopy [13,14] can reveal the anatomical skin description but fail in providing chemical specificity. In theory these imaging techniques can be combined with Raman spectroscopy [15] but the latter cannot provide active compounds images because of the very low molecular spontaneous Raman cross section that requires long pixel acquisition time (ms to s). Conversely, coherent Raman techniques [16,17] such as coherent anti-Stokes Raman scattering (CARS) microscopy [18] and stimulated Raman scattering (SRS) [19,20] can provide fast chemically specific

* Corresponding author at: Hervé Rigneault, Institut Fresnel, Domaine Univ St Jérôme, 13397 Marseille, Cedex 20, France.
E-mail address: herve.rigneault@fresnel.fr (H. Rigneault).

https://doi.org/10.1016/j.jconrel.2019.07.018
Received 1 February 2019; Received in revised form 4 July 2019; Accepted 14 July 2019
Available online 15 July 2019

images due to the coherent addition of the radiated fields scattered by chemical bonds [21]. CARS and SRS have been applied to image skin and drug delivery to skin [22–27], however active molecule concentrations with depth couldn't be quantified. We recently filled this gap using CARS that has the ability to provide unbiased in-depth concentration map, by correcting for the signal attenuation with increasing depth into the skin sample ex vivo [28]. However, this active molecule quantification in skin focused on ex vivo samples and potentially missed the contributions from living skin such as sweating and active metabolic contribution to percutaneous penetration. Indeed, using CARS imaging we have recently reported in vivo sweat pore activity and monitor the water production at a single sweat pore level [29], this aqueous sweat addition found in living skin affects active molecule percutaneous penetration and motivates further in vivo studies such as the one reported here.

In this paper, the use of deuterated active molecular compounds was combined together with CARS and two-photon excited auto-fluorescence (TPEF) to study in vivo percutaneous penetration of deuterated glycerol diluted in vehicles such as water and xanthan gel. The focus on glycerol was chosen as it is a major molecule involved in skin hydration. It has been shown previously that glycerol applied topically is responsible for skin hydration [30,31] but can also accelerate the recovery of the skin barrier function [32]. In the cosmetic industry moisturizing products extensively using glycerol to control the stratum corneum (SC) thickness, hydration and mechanical properties [33–35]. In vivo 3D quantitative glycerol mapping in human forearms are here provided and followed over several hours. We found that the glycerol distribution over time is maintained when diluted into xanthan gel, the latter acting as a glycerol reservoir on the skin surface. It was also found that the SC thickness is affected depending on the vehicle.

2. Results

2.1. In vivo quantitative CARS imaging method

To perform an in vivo active molecule imaging on the forearm of a Caucasian healthy subject several innovations were designed and implemented that are reviewed and detailed below (Fig. 1).

2.1.1. λ-switch CARS detection

Because the CARS signal is hampered by a non-resonant background that leads to potential spectral [36] and spatial artifacts [37] we have implemented the 'λ-switch' imaging scheme that performs sequential image acquisitions at the 2100 cm^{-1} carbon deuterium (C-D) vibrational frequency, referred as the resonant (R) CARS signal I_R, and at 2250 cm^{-1}, a vibrational frequency that does not correspond to the resonant C-D bond, and referred as the nonresonant (NR) CARS signal I_{NR}. The approach is similar to earlier and recent faster FM-CARS developments [38,39]. Here to perform the I_R and I_{NR} sequential acquisitions a specific 3 colors CARS setup was implemented, based on a frequency doubled ytterbium laser pumping two optical parametric oscillators (Fig. S1). The system provides 1.5 ps pulses trains at 80 MHz, up to 300 mW power at the sample plane for each of the 1031 nm, 847 nm and 837 nm beams. Using mechanical shutters to open and close sequentially the 847 nm and 837 nm laser beams, we measure sequentially I_R and I_{NR} at a fixed depth z and over 100 µm × 100 µm field of view in < 10 s. This is fast enough to avoid the artifact related to slow movements of the forearm (Fig. 1 a ①). The imaging process is then repeated at another depth z to acquire an in depth 3D image stack.

2.1.2. Balancing R and NR CARS signal on in vivo skin

To use $I_{NORM} = (I_R - I_{NR})/I_{NR}$ as a quantitative measurement of deuterated glycerol concentration in skin the 847 nm (OPO1) and 837 nm (OPO2) beam powers were adjusted to obtain equal 2100 cm^{-1} (I_R) and 2250 cm^{-1} (I_{NR}) CARS signals on a forearm treated with water only. This ensures that I_R and I_{NR} are equal on in vivo samples when no active molecules are present. To address the variation of I_{NORM} with deuterated glycerol concentration we conduct in vitro calibration tests where $I_{NORM} = (I_R - I_{NR})/I_{NR}$ was recorded with the deuterated glycerol concentration in water (Fig. S2). For concentration below 50% mass, we found that I_{NORM} scales linearly with the deuterated glycerol concentration. This is why in this regime, and using relatively short pulses, the CARS signal is dominated by the nonresonant background [28,40] (Sup Info section 7). The assumption was made that this linear dependence also holds for in vivo samples as I_{NR} is found to be stronger in skin than in solution. Altogether we will work with the hypothesis that I_{NORM} is a linear reporter of deuterated glycerol concentration in skin,

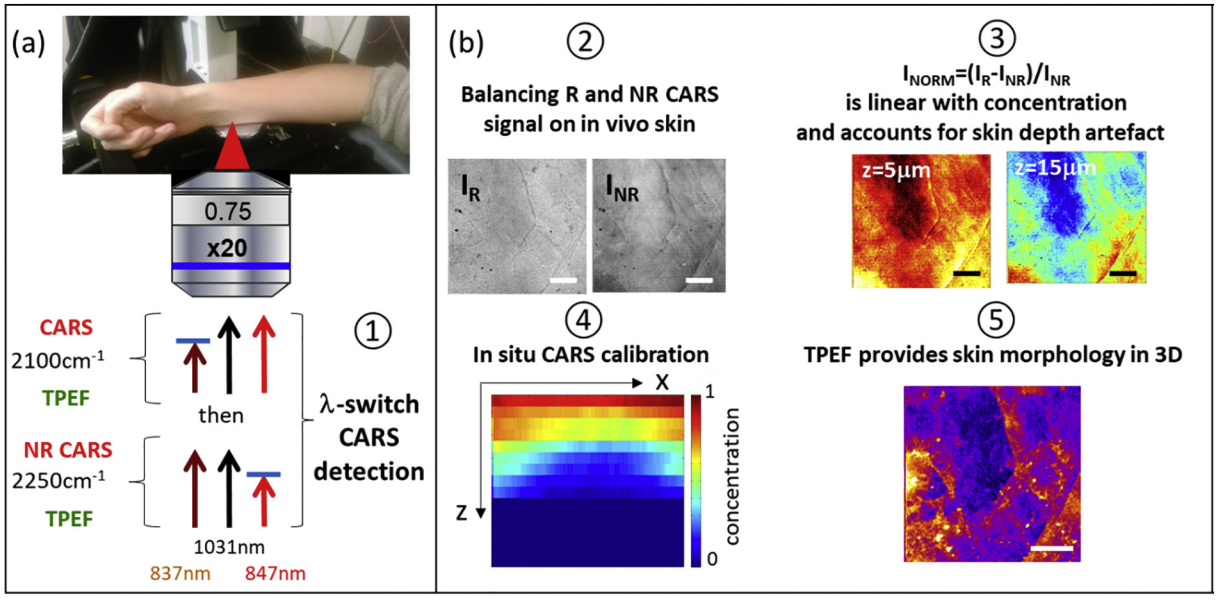

Fig. 1. Designed CARS and TPEF imaging framework for in vivo percutaneous penetration in human skin forearm. (a) λ-switch scheme to image sequentially deuterated molecular compounds (2100 cm^{-1}) and CARS non resonant background (2250 cm^{-1}) ①, (b) balancing the CARS resonant I_R (2100 cm^{-1}) and non-resonant I_{NR} (2250 cm^{-1}) ② signals, enables to build $I_{NORM} = (I_R\text{-}I_{NR})/I_{NR}$ that is linear with concentration and insensitive to skin depth artifact ③, in situ CARS calibration using the applied active molecule solution (as accumulated on surface wrinkles) ④ and TPEF images ⑤ enable to access 3D active deuterated molecule concentration in human skin in vivo.

in vivo, provided that I_R and I_{NR} CARS signals have been balanced on a forearm treated with water only (Fig. 1 b ②). Note that also we observe here a linear dependence of the CARS signal with concentration CARS is usually quadratic with concentration, this is potentially not a problem but it should be accurately calibrated [28].

2.1.3. I_{NORM} accounts for light scattering and attenuation in skin in vivo

In [28] the CARS nonresonant background was used to account for the loss of excitation and collection efficiency along the sample depth z. This is because I_{NR} should be constant with increasing depth in an ideal sample without light scattering and attenuation. On a forearm I_{NR} is found to decrease for increasing depth to eventually reach zero at z∼50 μm (Fig. S3), this is because at this depth skin scattering and absorption limit CARS signal activation and collection. $I_{NORM}(z) = (I_R(z)\text{-}I_{NR}(z))/I_{NR}(z)$ is therefore representative of the deuterated glycerol concentration with depth z as being renormalized by the nonresonant background attenuation (Fig. 1 b ③). We note that a similar strategy using cross phase modulation has been used to perform background free hyperspectral stimulated Raman scattering (SRS) spectroscopy [41].

2.1.4. In situ CARS calibration

Calibration of coherent Raman signals (CARS, SRS) is always an issue as the signal is very dependent on power but also spatial and temporal overlap of pump and Stokes beams. We adopt here in situ calibration using a measurement point in the sample where the deuterated glycerol concentration is known. This is possible when wrinkles are present on skin surface that tend to accumulate the applied deuterated glycerol solution. As an example, Fig. S4 shows a representative wrinkle at the skin surface where the deuterated glycerol accumulates. We assume that the deuterated glycerol concentration at these accumulation areas is the known applied glycerol concentration such that, it is possible to rescale the full I_{NORM} (x,y,z) image stack taking advantage of the CARS signal linearity with concentration (Fig. 1 b ④ and Fig. S2).

2.1.5. TPEF provides skin morphology in 3D

Independent to CARS, the identification of skin morphology (wrinkles, skin surface, skin layer compartments) in 3D is provided by two-photon excited auto-fluorescence (TPEF) (Fig. 1 b ⑤). For instance skin surface is usually associated to a strong in plane (x,y) integrated TPEF signal but also to a maximal in plane spatial variance (on the skin surface the TPEF intensity fluctuates a lot because of skin morphology irregularities).

2.2. In vivo glycerol percutaneous penetration

Using the methodology described above, the percutaneous penetration of deuterated glycerol was investigated in vivo, and the differences were compared when it is diluted at 40% (mass.) in two vehicles water and xanthan gel (Fig. S5), labeled as G_{wat} and G_{xant}, respectively. 30 μL of the formulations G_{wat} and G_{xant} are applied on the skin surface at $T = 0$ (see Materials and Methods) and the penetration of glycerol is followed kinetically in space and time in the skin. Fig. 2 shows examples of TPEF and glycerol concentration recording with increasing depth taken at $T = 1$ h after the topical application of G_{wat} (Fig. 2 a) and G_{xant} (Fig. 2b). In both cases, TPEF images reveal the stratum corneum (SC) corneocytes and enable to locate the skin surface using the maximum of the in plane (x,y) integrated TPEF signal variance with depth z (data not shown). The CARS images permit one to retrieve the deuterated glycerol concentration with depth, where the concentration is normalized to 1 for a bulk solution (40% mass.). Besides, glycerol concentration profile (in plane (x,y) integration) with increasing depth is presented in the right panels in Fig. 2 a b. Contrarily to formula G_{wat} (Fig. 2 a), formula G_{xant} reveals a higher glycerol concentration on the skin surface (Fig. 2b). This can be also quantitatively evaluated by comparing glycerol penetration profiles at the skin surface (< 5 μm). However, in both cases the glycerol concentration drops with increasing depth, and reaches the concentration detection limit at ∼15 μm.

To gain more insights on the glycerol percutaneous diffusion process, Fig. 3 shows time lapse (x,z) glycerol concentration images where the glycerol concentration has been integrated along y axis (1 corresponds to a glycerol concentration of 40%). The probed areas are in the same vicinity on the forearm (within ∼1mm^2) during a time lapse experiment. In the case of formulation G_{wat}, (Fig. 3 a) glycerol concentration tends to decrease rapidly from the skin surface (Fig. 3 c – blue dots) eventually reaching a close to zero skin surface concentration at $T = 4$ h. Such a result is compatible with glycerol remanence time in skin which is of the order of a few hours [33]. On the contrary, in the case of formulation G_{xant} (Fig. 3 b) our measurements reveal the creation of a glycerol reservoir on the skin surface and a much higher glycerol mean concentration in the upper part of the SC ($T < 2$ h, 0–10 μm depth) as compared to formulation G_{wat} (Fig. 3 b). This glycerol accumulation also results in stronger glycerol remanence into the SC depth, for instance at T = 4 h the glycerol concentration is still ∼20% at z = 10 μm whereas it is non-detectable in the case of formulation G_{wat}. In both cases the glycerol spatial penetration is quite homogeneous, although areas of stronger diffusion with depth can appear, these results are consistent with our previous ex vivo study [28]. The presented results were obtained on a 30 years old Caucasian woman volunteer (Fig. S6).

To further quantify the percutaneous penetration of deuterated glycerol diluted in water and xanthan gel we concentrate on the concentration profiles with increasing depth. Example of such traces are shown as insets in Fig. 3 c for formulations G_{wat} and G_{xant}. With xanthan gel (G_{xant}), the profile at shorter exposure time is nonlinear and becomes linear at higher exposure time (> 1 h10). Lack of linearity over the exposure time with aqueous solution can be explained by the difficulty to control the skin exposure to G_{wat}. Despite these uncertainties, all data were fitted through a linear regression (Fig. 4 a). Around 30 concentration profiles (acquired at different locations on the forearm), averaged every 5 min and acquired at different times T (every 8 min from 10 min to 240 min) after topical applications of the formulations G_{wat} and G_{xant} on the skin surface, exhibit this linear behavior. At short exposure time (< 60 min), A is not constant and increased over the time (Fig. 4 b). Then, it remains constant up to 3 h. The slopes $A(T)$ (negative slop) for both formulations are very similar (blue empty triangles and red empty squares Fig. 4 b). Conversely the evolutions of the deuterated glycerol concentration at the skin surface $C_0(T)$ are different for the two formulations. For G_{wat}, $C_0(T)$ shows a sharp drop between $T = 0$ and $T = 60$ min and reaches a plateau close to the ∼10% concentration detection limit. On the contrary, for G_{xant}, $C_0(T)$ remains constant and close to ∼30%–40% until $T = 180$ min. At steady state, both values A and C_0 have to be constant over the time. At shorter exposure time (< 60 min), steady state is not reached. At longer exposure time, steady state is not obtained for G_{wat} as C_0 decreases over time. Steady state is obtained with G_{xant} as supported by constant A and C_0 values and the linear profile at 1 h10 (Fig. 3c). This is a clear indication that the xanthan gel acts as a reservoir at the skin surface and retains the deuterated glycerol up to 3 h, enhancing its remanence as compared to the water vehicle.

For the 3D TPEF stack it is possible to quantify the stratum corneum (SC) thickness following the application of the formulations (Fig. 4 c d). This has been done visually from the TPEF image stacks for every time T, looking at the depth range where the corneocytes are clearly distinguishable (data not shown). This visual inspection could immediately reveal that the corneocyte shapes are different and more swollen for the xanthan gel formulation (G_{xant}) as compared to the water formulation (G_{wat}) (Fig. 4c). Fig. 4 d shows the SC thickness evolution with time T during the deuterated glycerol penetration for both formulations. Note that the experiments were performed on different areas on the forearm. Both formulations tend to induce SC

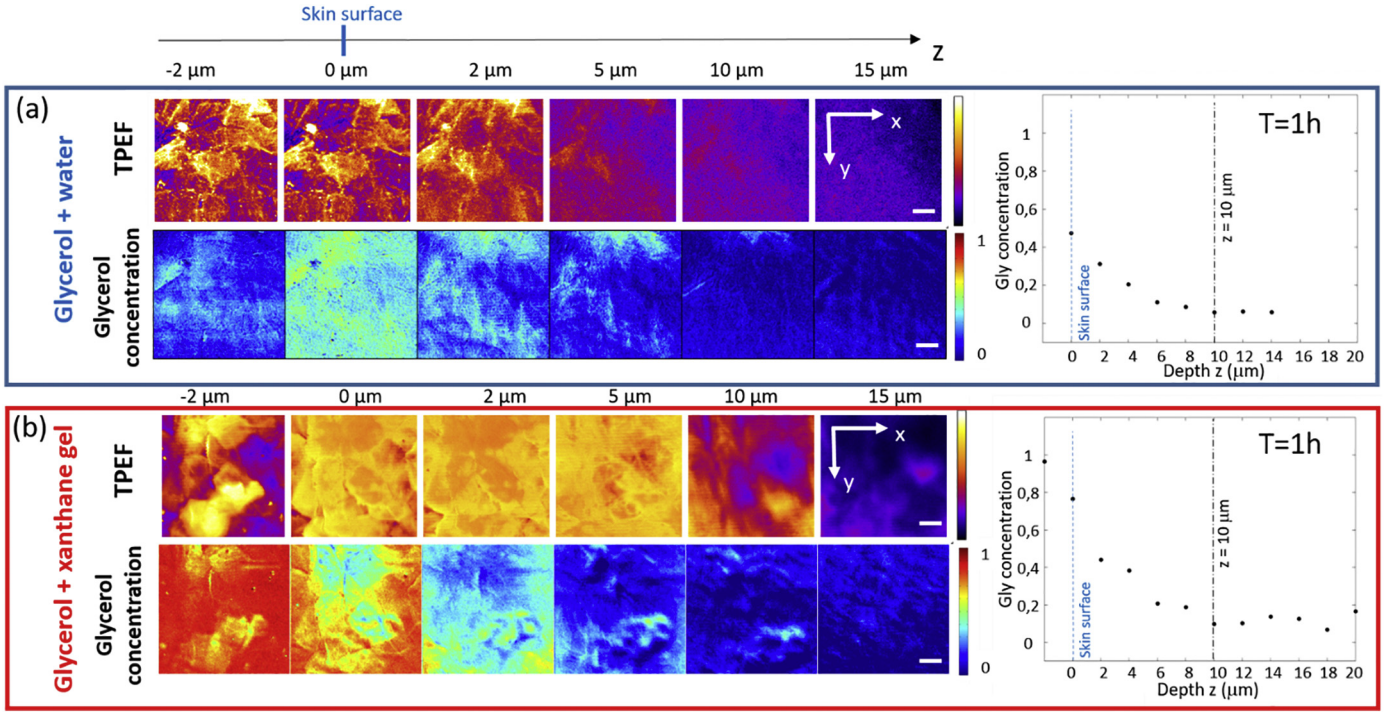

Fig. 2. In vivo TPEF and deuterated glycerol concentration in human forearm with increasing depth $T = 1$ h after the application of 30 µL of formulation on the skin surface. Deuterated glycerol is diluted at 40% (mass) into water (formulation G_{wat}) (a) and xanthan gel (formulation G_{xant}) (b). TPEF images with depth z enable to visualize the corneocytes and to locate the skin surface. The graphs on the right show the in plane (x,y) integrated deuterated glycerol concentration with depth z. Xanthan gel retains a glycerol reservoir on the skin surface. Glycerol concentration: 1 corresponds to a concentration of 40% mass. TPEF images are in arbitrary unit. Scale bar: 20 µm.

swelling between $T = 0$ and $T = 220$ min. However this swelling is 1.5 more prominent in the case of G_{xant} than G_{wat} (30% and 50% swelling in the case of G_{wat} and G_{xant}, respectively). This result is consistent with the larger corneocyte shape initially observed in the case of G_{xant} (Fig. 4c).

3. Discussion

CARS has been used throughout this work to perform deuterated glycerol concentration map in human skin in vivo. This has been possible because (1) deuterated glycerol at 40%–10% concentration provides a viable *epi* detected CARS signal when topically applied on human skin and (2) the nonresonant CARS background provides a ruler for the excitation pump and Stokes beams attenuation and scattering with increasing skin depth. Contrary to CARS our attempts to use SRS failed because the reflected deuterated glycerol SRS signal from human skin was to weak and the SRS contrast doesn't provide a nonresonant background for in depth normalization purposes.

Using CARS, our results demonstrate that the in vivo percutaneous penetration of glycerol into human skin is confirmed to be affected by the vehicle (water or xanthan gel). The compositions of cosmetic formulations indeed play an important role into skin bio-distribution and the imaging framework presented here provides a way to visualize and quantify how deuterated active molecules penetrate into skin in vivo. Our measurements clearly indicate that xanthan gel retains glycerol on the skin surface over time (Fig. S8) and enables its continuous delivery to skin over a time frame that is at least twice that of the water vehicle (2 h for water vehicle versus 4 h for xanthan gel, z = 10 µm).

Although the glycerol initial concentration (40%, w/w) is the same on the skin surface and the application protocol identical for both vehicles, it is more challenging to control the spreading of water vehicle as compared to xanthan gel. This is because of both the more viscous nature of the xanthan gel and the skin hydrophobicity. Therefore, we cannot rule out the fact that the glycerol diluted in water might spread over a larger skin area as compared to the xanthan gel and exhibits slightly lower surface concentration. Such a situation further validates the fact that xanthan gel acts as a 'robust' glycerol reservoir located at the skin surface enabling the release of active molecule in the long run. Indeed, up to 2 h after application the xanthan gel moisture is still preset on the skin surface whereas it disappears for the water vehicle within minutes.

We showed a SC thickness prominent increase for the xanthan gel vehicle that is also clearly noticeable on the TPEF images. Indeed, the corneocytes are clearly swollen at 1 h on Fig. 4 c. This is to be related to the known homogeneous glycerol diffusion through skin that is enhanced with the xanthan gel vehicle.

When compared with our previous work on glycerol penetration in ex vivo skin samples, our present findings on the forearm show that steady state in vivo is achieved in ~1 h, especially in the case of the xanthan vehicle (G_{xant}) as revealed by the linear deuterated glycerol concentration profile (Fig. 3 c and Fig. 4 a b). This is different from the results obtained on ex vivo skin abdominal sample where transient diffusion was still observed after 4 h and steady state diffusion was recorded after 24 h in an infinite dose scheme (Fig. S6 from [28]). Beside the differences between samples (forearm in vivo and abdomen ex vivo) and formula (xanhan gel with finite dose vs aqueous solution in infinite dose) we conclude that living skin (metabolism, sweating, sebum, microbiota…) accelerates the percutaneous penetration of deuterated glycerol in skin showing that in vivo bio-availability is different than ex vivo.

Although our λ-switch modality requires 20 s (I_R and I_{NR}) to image a 100 µm field of view, leading to 5 min acquisition time for a 100 µm × 100 µm × 30 µm volume, the calibration process time on a wrinkle, together with the accurate positioning on a wrinkle free area requires ~15 min total which precludes studies of fast diffusing species. Recent development using fast modulation [42] or multifocus [43,44] should enable to reduce the acquisition speed by one order of magnitude.

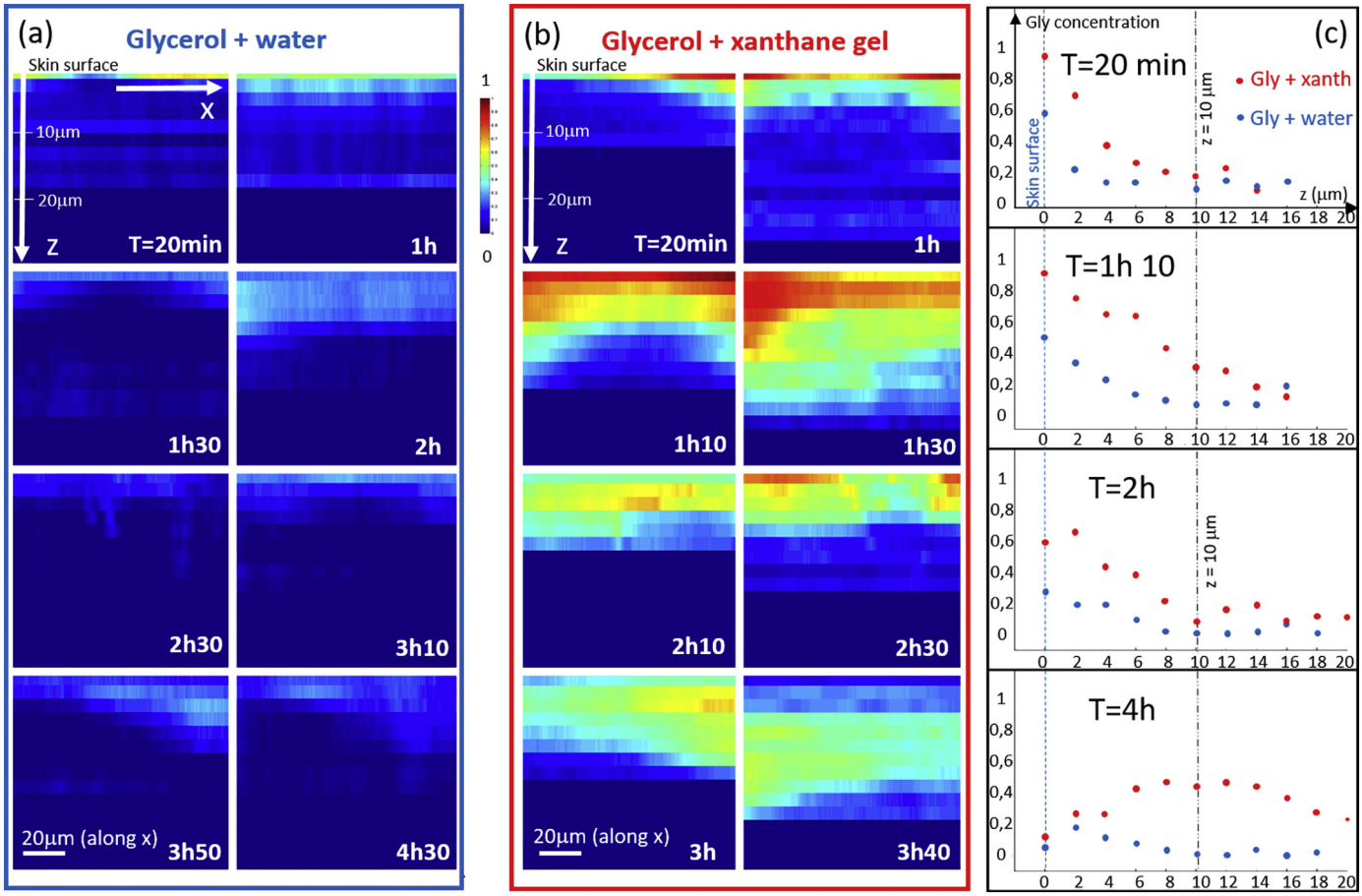

Fig. 3. In vivo time lapse glycerol percutaneous penetration after the application at $T = 0$ of 30 µL of formulation on the skin surface. Deuterated glycerol is diluted at 40% (mass) into water (formulation G_{wat}) (a) and xanthan gel (formulation G_{xant}) (b). (c) In plane (x,y) integrated deuterated glycerol concentration evolution in time for G_{wat} (blue dots) and G_{xant} (red dots). Glycerol concentration: 1 corresponds to a concentration of 40%. In (a) and (b) note that scale bars are not the same along x and z axis. (For interpretation of the references to colour in this figure legend, the reader is referred to the web version of this article.)

The λ-switch modality can detect a glycerol concentration of ~1% in solution (Fig. S2), however, the detection limit in vivo is of the order of ~10% due to noise and uncertainties. Indeed, our normalization process makes the CARS signal linear with the concentration but remains dependent on the nonresonant CARS susceptibility (see Sup Info section 7). We found that our assumption of a constant nonresonant CARS susceptibility in skin is valid within 10% (Fig. S9) and this sets our concentration precision and ultimate sensitivity. Furthermore, we have shown previously [28] that this limitation doesn't preclude the CARS quantification of active deuterated molecule in ex vivo excised skin as good agreement was found when compared with adhesive tape stripping followed by chromatography–tandem mass spectrometry analyses (LC–MS/MS). Note also that glycerol sometimes accumulates in patches in the skin and that the 10% stands for the spatially averaged concentration. This is a limitation to study active molecule that are commercially formulated with concentrations below 5%. A possible improvement would be to take advantage of faster FM-CARS modulation schemes [38,39] or the possible two photon absorption of active molecule to increase the coherent Raman cross section by one order of magnitude [45].

4. Conclusion

We have designed a multiphoton imaging framework based on two-photon induced auto-fluorescence (TPEF) and coherent anti-Stokes Raman scattering (CARS) that is able to monitor the skin morphology together with deuterated active molecule percutaneous penetration in human skin in vivo. Our λ-switch modality probes both the C-D resonant and nonresonant CARS signals for increased sensitivity and is insensitive to the scattering and attenuation of the excitation beams with increasing skin depth as using the CARS non resonant background as a correction ruler. With this tool, we have quantified the percutaneous penetration in vivo of deuterated glycerol diluted in two vehicles, water and xanthan gel. We found that contrary to water, xanthan gel vehicle retains glycerol on the skin surface over time enabling its constant release in the long run. We could also measure that the stratum corneum thickness increases more with the xanthan gel vehicle as compared to the water case. This results highlight the critical role of the vehicle and its ability for effective dermal delivery. The developed multiphoton imaging platform provides a nondestructive tool with chemical sensitivity to investigate cosmetic active molecule and pharmaceutical drug penetration into human skin in vivo. We believe the technology can be used to optimize active molecule design and their formulations for optimal skin bioavailability. Ultimately such a TPEF CARS imaging framework could be extended in handheld probes [46] or fiber endoscopes [47] to monitor active molecule penetration in inaccessible locations at the skin surface.

5. Materials and methods

5.1. 'λ-switch' nonlinear imaging

TPEF and CARS microscope images was performed on a custom setup (Fig. S1) using two optical parametric oscillators (OPOs)

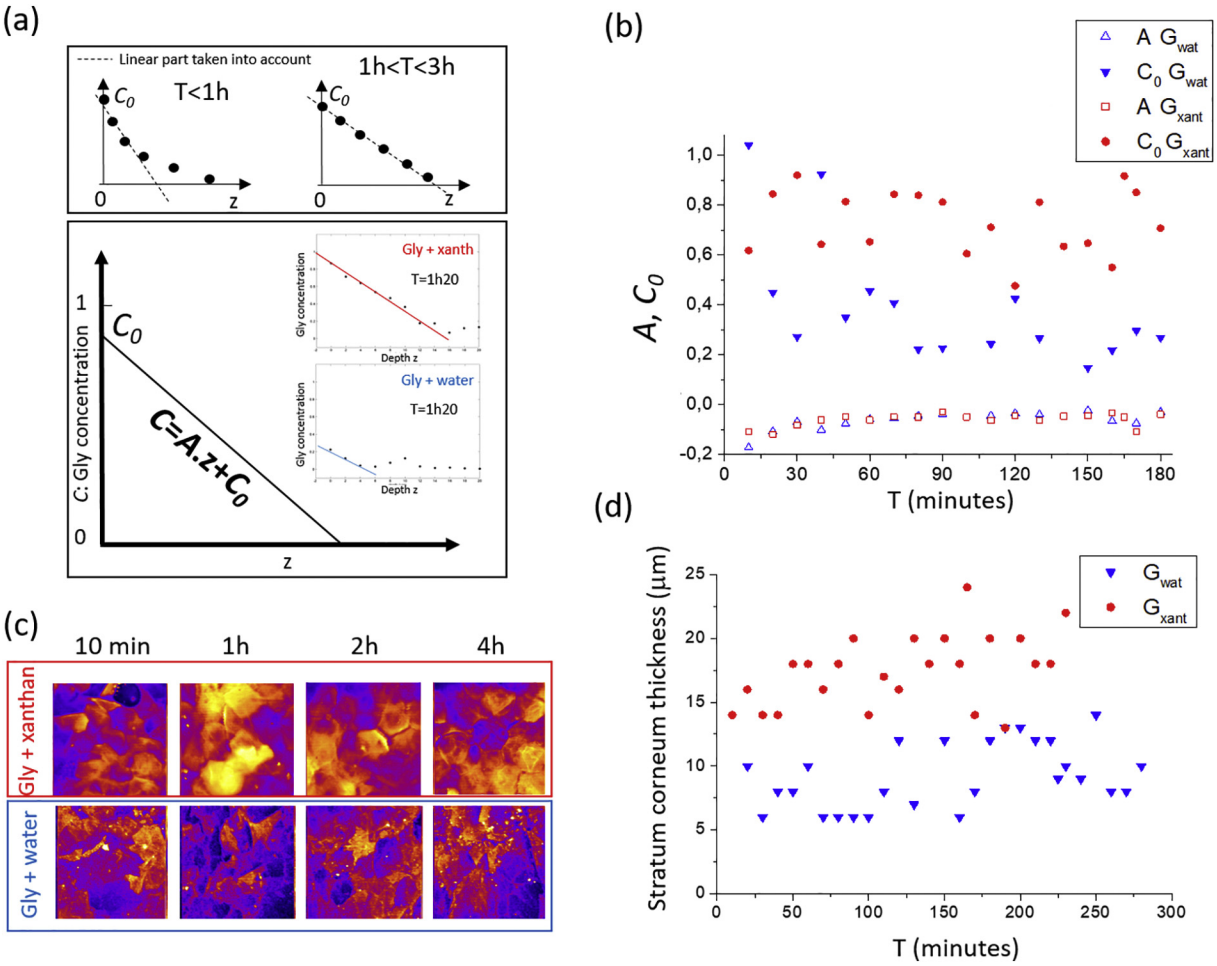

Fig. 4. Evolution of deuterated glycerol concentration and stratum corneum (SC) thickness after topical application time T. (a) A linear regression is used to fit concentration profiles with depth for both water and xanthan gel formulations (insets). (b) Evolution of concentration profile slopes *A* and surface concentration C_0 with time T, highlighting a surface reservoir created by the xanthan gel. (c) SC TPEF images versus T and (d) SC thickness evolution with time T.

(Emerald, APE) pumped by a frequency doubled Yb fiber laser (Emerald Engine, APE) operating at 516 nm. This 3 colors tunable system provides 1.5 ps pulses at 80 MHz repetition rate at wavelengths 1031 nm, 847 nm and 837 nm suitable to image the carbon deuterium vibration at 2100 cm^{-1} and the nonresonant background at 2250 cm^{-1}. The 3 beams are recombined using dichroic filters (D) and send to galvo mirrors (Cambridge Technology) prior their injection into an invested microscope(TiU, Nikon). The objective lens (Nikon, x20 NA = 0.75) can be translated along the z axis to focus the beams at various depth in the sample thanks to piezo scanner (PiFoc, PI). The CARS, TPEF signals are detected in the *epi* direction thanks to photomultiplier tubes (Hamamatsu, H7421–50 for CARS and H7421–40 for TPEF). A dedicated software written in Labview controls the systems including the OPOs [48].

For each depth, the resonant carbon deuterium (C-D) and nonresonant CARS images are acquired following the sequential obstruction of the OPO beams (Fig. S1 – inset) using mechanical shutters S1 and S2. This 'λ-switch' modality enables to acquire both 2100 cm^{-1} and 2250 cm^{-1} images over a 100 µm field of view and at a specific depth in 20s, a time short enough to minimize the movement of the forearm on the microscope stage. At the same time TPEF images are acquired. The imaging process is repeated at a different depth thanks to the piezo scanner.

Imaging conditions: 100 µm × 100 µm (200 × 200 pixels) (3 accumulations) images are acquired in 10 s (20 s for both 2100 cm^{-1} and 2250 cm^{-1}), performing z scan each 2 µm over 30 µm depth enables to acquire a full 3D λ-switch stack in 5 min. The power is set to 35 mW at the sample plane for each pump and Stokes beams.

5.2. *In vivo human forearm imaging*

The protocol follows closely the one reported in [29]. Briefly, the right forearm of the volunteer is cleaned with water and a region is delineated where a glass coverslip (diameter 25 mm, thickness 150 µm) is positioned directly on the skin. A custom-made metallic holder featuring a 20 mm clear aperture is firmly attached to the skin using doubled-sided adhesive so that the glass coverslip fits into its aperture. The glass coverslip flattens the skin surface and eases the image acquisition. The hand together with its holder is then securely fixed on the microscope stage with magnets for in vivo imaging, and the volunteer's right elbow is maintained (Fig. 1).

5.3. *Formulations and skin topical application*

Deuterated glycerol (purity > 99.5% - Sigma) is diluted at 40% (mass.) in two vehicles: pure water (G_{wat}) and 1% xanthan gel in pure water (G_{xant}). 30 µL of formulation is applied on the volunteer forearm in an area of 3 cm^2 (dose = 10 µl/cm^2), rubbed for 3 min with finger and left in open air for 2 min before being covered by a glass cover slip (occlusive condition for at least 1 h30). A 30 years old volunteer Caucasian women kindly participated in this study (Fig. S6).

Credit author statement

B.S., R.C., X.C. performed the experiments. X.C., S.B., F.F., J.B.G., A.P., T.B. and H.R. designed the research. All authors analyzed the results and wrote the manuscript.

Declaration of Competing Interest

The authors state no conflict of interest.

Acknowledgements

The authors acknowledge financial support the Centre National de la Recherche Scientifique (CNRS), France Aix-Marseille University (ANR-11-IDEX- 0001-02), France and ANR, France grants France Bio Imaging (ANR-10-INSB-04-01) and France Life Imaging (ANR-11-INSB-0006) infrastructure networks.

Appendix A. Supplementary data

Supplementary data to this article can be found online at https://doi.org/10.1016/j.jconrel.2019.07.018.

References

[1] E. Proksch, J.M. Brandner, J.M. Jensen, The skin: an indispensable barrier, Exp. Dermatol. 17 (2008) 1063–1072.
[2] M.R. Prausnitz, R. Langer, Transdermal drug delivery, Nat. Biotechnol. 26 (2008) 1261–1268.
[3] Y. Dancik, M.A. Miller, J. Jaworska, G.B. Kasting, Design and performance of a spreadsheet-based model for estimating bioavailability of chemicals from dermal exposure, Adv. Drug Deliv. Rev. 65 (2013) 221–236.
[4] J.A. Bouwstra, P.L. Honeywell-Nguyen, G.S. Gooris, M. Ponec, Structure of the skin barrier and its modulation by vesicular formulations, Prog. Lipid Res. 42 (2003) 1–36.
[5] F. Hueber-Becker, G.J. Nohynek, W.J. Meuling, F. Benech-Kieffer, H. Toutain, Human systemic exposure to a [14C]-para-phenylenediamine-containing oxidative hair dye and correlation with in vitro percutaneous absorption in human or pig skin, Food Chem. Toxicol. 42 (2004) 1227–1236.
[6] F.F. Sahle, S. Lange, B. Dobner, J. Wohlrab, R.H. Neubert, Development and validation of LC/ESI-MS method for the detection and quantification of exogenous ceramide NP in stratum corneum and other layers of the skin, J. Pharm. Biomed. Anal. 60 (2012) 7–13.
[7] C. Herkenne, I. Alberti, A. Naik, Y.N. Kalia, F.X. Mathy, V. Preat, R.H. Guy, In vivo methods for the assessment of topical drug bioavailability, Pharm. Res. 25 (2008) 87–103.
[8] P.J. Caspers, G.W. Lucassen, E.A. Carter, H.A. Bruining, G.J. Puppels, In vivo confocal Raman microspectroscopy of the skin: noninvasive determination of molecular concentration profiles, J. Invest. Dermatol. 116 (2001) 434–442.
[9] F.D. Fleischli, S. Mathes, C. Adlhart, Label free non-invasive imaging of topically applied actives in reconstructed human epidermis by confocal Raman spectroscopy, Vib. Spectrosc. 68 (2013) 29–33.
[10] D. Mohammed, P.J. Matts, J. Hadgraft, M.E. Lane, In vitro-in vivo correlation in skin permeation, Pharm. Res. 31 (2014) 394–400.
[11] S. El Gammal, C. El Gammal, K. Kaspar, C. Pieck, P. Altmeyer, M. Vogt, H. Ermert, Sonography of the skin at 100 MHz enables in vivo visualization of stratum corneum and viable epidermis in palmar skin and psoriatic plaques, J. Investigat. Dermatol. 113 (1999) 821–829.
[12] J. Welzel, E. Lankenau, R. Birngruber, R. Engelhardt, Optical coherence tomography of the human skin, J. Am. Acad. Dermatol. 37 (1997) 958–963.
[13] X. Liang, B.W. Graf, S.A. Boppart, In vivo multiphoton microscopy for investigating biomechanical properties of human skin, Cell. Mol. Bioeng. 4 (2011) 231–238.
[14] Y. Zhao, B.W. Graf, E.J. Chaney, Z. Mahmassani, E. Antoniadou, R. Devolder, H. Kong, M.D. Boppart, S.A. Boppart, Integrated multimodal optical microscopy for structural and functional imaging of engineered and natural skin, J. Biophotonics 5 (2012) 437–448.
[15] C.A. Patil, H. Kirshnamoorthi, D.L. Ellis, T.G. van Leeuwen, A. Mahadevan-Jansen, A clinical instrument for combined Raman spectroscopy-optical coherence tomography of skin cancers, Lasers Surg. Med. 43 (2011) 143–151.
[16] C.H. Camp Jr, M.T. Cicerone, Chemically sensitive bioimaging with coherent Raman scattering, Nat. Photonics 9 (2015) 295–305.
[17] H. Rigneault, P. Berto, Tutorial: coherent Raman light matter interaction processes, APL Photonics 3 (2018) 091101.
[18] A. Zumbusch, G.R. Holtom, X.S. Xie, Vibrationnal microscopy using coherent anti-stokes Raman scattering, Phys. Rev. Lett. 82 (1999) 4014–4017.
[19] C.W. Freudiger, W. Min, B.G. Saar, S. Lu, G.R. Holtom, C. He, J.C. Tsai, J.X. Kang, X.S. Xie, Label-free biomedical imaging with high sensitivity by stimulated Raman scattering microscopy, Science 322 (2008) 1857–1861.
[20] P. Nandakumar, A. Kovalev, A. Volkmer, Vibrational imaging based on stimulated Raman scattering microscopy, New J. Phys. 11 (2009) 033026.
[21] J.X. Cheng, S. Xie, Coherent Raman Scattering Microscopy, CRC Press, 2013.
[22] B.G. Saar, L.R. Contreras-Rojas, X.S. Xie, R.H. Guy, Imaging drug delivery to skin with stimulated Raman scattering microscopy, Mol. Pharm. 8 (2011) 969–975.
[23] N.A. Belsey, N.L. Garrett, L.R. Contreras-Rojas, A.J. Pickup-Gerlaugh, G.J. Price, J. Moger, R.H. Guy, Evaluation of drug delivery to intact and porated skin by coherent Raman scattering and fluorescence microscopies, J. Control. Release 174 (2014) 37–42.
[24] H.G. Breunig, R. Bückle, M. Kellner-Höfer, M. Weinigel, J. Lademann, W. Sterry, K. König, Combined in vivo multiphoton and CARS imaging of healthy and disease-affected human skin, Microsc. Res. Tech. 75 (2012) 492–498.
[25] K. Koenig, Hybrid multiphoton multimodal tomography of in vivo human skin, IntraVital 1 (2012) 11–26.
[26] C.L. Evans, E.O. Potma, M. Puoris'haag, D. Cote, C.P. Lin, X.S. Xie, Chemical imaging of tissue in vivo with video-rate coherent anti-Stokes Raman scattering microscopy, Proc. Natl. Acad. Sci. U. S. A. 102 (2005) 16807–16812.
[27] B.G. Saar, C.W. Freudiger, J. Reichman, C.M. Stanley, G.R. Holtom, X.S. Xie, Video-rate molecular imaging in vivo with stimulated Raman scattering, Science 330 (2010) 1368–1370.
[28] X. Chen, S. Grégoire, F. Formanek, J.-B. Galey, H. Rigneault, Quantitative 3D molecular cutaneous absorption in human skin using label free nonlinear microscopy, J. Control. Release 200 (2015) 78–86.
[29] X. Chen, P. Gasecka, F. Formanek, J.B. Galey, H. Rigneault, In vivo single human sweat gland activity monitoring using coherent anti-Stokes Raman scattering and two-photon excited autofluorescence microscopy, Br. J. Dermatol. 174 (2016) 803–812.
[30] K. Levi, A. Kwan, A.S. Rhines, M. Gorcea, D.J. Moore, R.H. Dauskardt, Effect of glycerin on drying stresses in human stratum corneum, J. Dermatol. Sci. 61 (2011) 129–131.
[31] S.A. Ventura, G.B. Kasting, Dynamics of glycerine and water transport across human skin from binary mixtures, Int. J. Cosmet. Sci. 39 (2017) 165–178.
[32] J.W. Fluhr, M. Gloor, L. Lehmann, S. Lazzerini, F. Distante, E. Berardesca, Glycerol accelerates recovery of barrier function in vivo, Acta Derm. Venereol. 79 (1999) 418–421.
[33] L. Chrit, P. Bastien, G.D. Sockalingum, D. Batisse, F. Leroy, M. Manfait, C. Hadjur, An in vivo randomized study of human skin moisturization by a new confocal Raman fiber-optic microprobe: assessment of a glycerol-based hydration cream, Skin Pharmacol. Physiol. 19 (2006) 207–215.
[34] J.M. Crowther, A. Sieg, P. Blenkiron, C. Marcott, P.J. Matts, R. Kaczvinsky, A.V. Rawlings, Measuring the effects of topical moisturizers on changes in stratum corneum thickness, water gradients and hydration in vivo, Br. J. Dermatol. 159 (2008) 567–577.
[35] J.W. Fluhr, R. Darlenski, C. Surber, Glycerol and the skin: holistic approach to its origin and functions, Br. J. Dermatol. 159 (2008) 23–34.
[36] H. Rigneault, D. Gachet, Background-free coherent Raman imaging: The CARS and SRS contrast mechanisms, in: A. Zoubir (Ed.), Raman Imaging, Springer-Verlag, Heidelberg, 2012, pp. 347–372.
[37] D. Gachet, F. Billard, N. Sandeau, H. Rigneault, Coherent anti-Stokes Raman scattering (CARS) microscopy imaging at interfaces: evidence of interference effects, Opt. Express 15 (2007) 10408–10420.
[38] F. Ganikhanov, C.L. Evans, B.G. Saar, X.S. Xie, High-sensitivity vibrational imaging with frequency modulation coherent anti-Stokes Raman scattering (FM CARS) microscopy, Opt. Lett. 31 (2006) 1872–1874.
[39] B. Sarri, X. Chen, R. Canonge, S. Grégoire, F. Formanek, J-B. Galey, AnnePotter, T. Bornschlögl, H. Rigneault, In vivo quantitative molecular absorption of glycerol in human skin using coherent anti-Stokes Raman scattering (CARS) and two-photon auto-fluorescence, Sci. Rep. (2019), https://doi.org/10.1016/j.jconrel.2019.07.018.
[40] H. Rigneault, P. Berto, Tutorial: coherent Raman light matter interaction processes, APL Photonics 3 (2018).
[41] M. Andreana, M.-A. Houle, D.J. Moffatt, A. Ridsdale, E. Buettner, F. Légaré, A. Stolow, Amplitude and polarization modulated hyperspectral stimulated Raman scattering microscopy, Opt. Express 23 (2015) 28119–28131.
[42] S. Heuke, B. Sarri, X. Audier, H. Rigneault, Simultaneous dual-channel stimulated Raman scattering microscopy demultiplexed at distinct modulation frequencies, Opt. Lett. 43 (2018) 3582–3585.
[43] S. Heuke, B. Sarri, A. Lombardini, X. Audier, H. Rigneault, Dual-focus stimulated Raman scattering microscopy: a concept for multi-focus scaling, Opt. Lett. 43 (2018) 4763–4766.
[44] F.B. Legesse, T. Meyer, S. Heuke, T. Gottschall, T. Pascher, J. Limpert, A. Tünnermann, M. Schmitt, J. Popp, Dual-focus coherent anti-stokes Raman scattering microscopy using a compact two-beam fiber laser source, Opt. Lett. 42 (2017) 183–186.
[45] L. Wei, Z. Chen, L. Shi, R. Long, A.V. Anzalone, L. Zhang, F. Hu, R. Yuste, V.W. Cornish, W. Min, Super-multiplex vibrational imaging, Nature 544 (2017) 465.
[46] C.-S. Liao, P. Wang, C.Y. Huang, P. Lin, G. Eakins, R.T. Bentley, R. Liang, J.-X. Cheng, In vivo and in situ spectroscopic imaging by a handheld stimulated Raman scattering microscope, ACS Phot. 5 (2018) 947–954.
[47] A. Lombardini, V. Mytskaniuk, S. Sivankutty, E.R. Andresen, X. Chen, J. Wenger, M. Fabert, N. Joly, F. Louradour, A. Kudlinski, H. Rigneault, High-resolution multimodal flexible coherent Raman endoscope, Light 7 (2018) 10.
[48] P. Ferrand, GPScan.VI: a general-purpose LabVIEW program for scanning imaging or any application requiring synchronous analog voltage generation and data acquisition, Comput. Phys. Commun. 192 (2015) 342–347.